Pramana – J. Phys. (2018) 90:27
https://doi.org/10.1007/s12043-018-1520-6

Optical characteristics of a RF DBD plasma jet in various Ar/O_2 mixtures

A FALAHAT[1], A GANJOVI[2,*], M TARAZ[1], M N ROSTAMI RAVARI[1] and A SHAHEDI[2]

[1]Faculty of Physics, Shahid Bahonar University of Kerman, Kerman, Iran
[2]Photonics Research Institute, Graduate University of Advanced Technology, Kerman, Iran
*Corresponding author. E-mail: ganjovi@kgut.ac.ir; alirezaganjovi@yahoo.com

MS received 21 July 2017; revised 15 September 2017; accepted 22 September 2017;
published online 25 January 2018

Abstract. In this paper, using the optical emission spectroscopy (OES) technique, the optical characteristics of a radiofrequency (RF) plasma jet are examined. The Ar/O_2 mixture is taken as the operational gas and, the Ar percentage in the Ar/O_2 mixture is varied from 70% to 95%. Using the optical emission spectrum analysis of the RF plasma jet, the excitation temperature is determined based on the Boltzmann plot method. The electron density in the plasma medium of the RF plasma jet is obtained by the Stark broadening of the hydrogen Balmer H_β. It is mostly seen that, the radiation intensity of Ar 4p→4s transitions at higher argon contributions in Ar/O_2 mixture is higher. It is found that, at higher Ar percentages, the emission intensities from atomic oxygen (O) are higher and, the line intensities from the argon atoms and ions including O atoms linearly increase. It is observed that the quenching of Ar^* with O_2 results in higher O species with respect to O_2 molecules. In addition, at higher percentages of Ar in the Ar/O_2 mixture, while the excitation temperature is decreased, the electron density is increased.

Keywords. Radiofrequency jet; plasma jet; optical emission spectroscopy; Ar/O_2 mixture.

PACS Nos 52.50.−b; 52.50.Dg; 52.77.−j; 52.75.−d; 52.70.−m

1. Introduction

In recent years, cold plasmas at atmospheric pressures have attracted much attention in various fields of science and technology [1–9]. The atmospheric pressure plasma discharges are practically used because of their simplicity and low cost [10]. To improve the efficiency of the plasma discharge jet for plasma processing, cold plasma with various mixtures of atomic and molecular gases is used. The plasma jet is used for medical applications such as surgery, blood coagulation, sterilisation, removal of bacteria, cancer therapy, dentistry and oncology [11–14]. In addition to the biomedical applications, various manufactured plasma jets based on the Ar/O_2 mixture discharges are widely used for oxidisation, formation of passivation layer, or other plasma technologies that are applicable for the production of integrated circuits [15,16].

Using optical emission spectroscopy (OES) scheme, the physical properties of a kHz-driven atmospheric plasma jet with the Ar/O_2 mixture at a low flow gas were examined by Moravsky *et al* [11]. Their plasma jet was used to inactivate *Candida albicans* cells which were in suspension in phosphate buffered saline.

The fundamental plasma characteristics of Ar/O_2 mixture gas plasma using the atmospheric pressure microwave plasma source was experimentally described by Ono *et al* [17]. They observed that the electron temperature and electron density are maximised at about 1.2 eV and 2.5×10^{16} cm^{-3}, respectively. Furthermore, a slight reduction in the electron density and temperature towards the centre of plasma column was reported.

Wagatsuma and Kichinosuke [18] reported the spectroscopic features of the Ar/O_2 mixture glow discharge plasma. They found that, for both pure argon and oxygen and at a pressure of 6.7×10^2 Pa, reduction in the discharge current at the oxygen plasma at lower applied voltages is more than that of the argon plasma. Interestingly, their results show that, when a small amount of oxygen is added, the discharge current and emission intensity in the argon plasma decrease immediately. However, at higher percentages of added oxygen, the threshold applied voltage increases and the emission intensity reduces.

Ying *et al* [19] studied an atmospheric pressure plasma jet generated by Ar and Ar/O_2 mixture as the background gases. Their plasma jet was specially designed based on double AC power electrodes at a frequency of 20–32 kHz and a fixed applied voltage of 8 kV. The increasing effects of discharge frequency on the power consumption and excitation temperature were observed.

Using the OES technique which was combined with an RF-compensated Langmuir probe, Chung *et al* investigated the physical characteristics of an inductively coupled plasma with argon, oxygen, and Ar/O_2 mixture [15]. It was reported that, the electron temperature decreases at higher input powers and gas pressures. Besides, it was seen that the electron temperature decreases with increasing Ar amount.

This study mainly focusses on different physical properties of the plasma discharge medium of the RF plasma jet such as temperature and density of the plasma electrons. However, owing to these physical properties and the mechanisms for creation of the excited energy states and so on, different types of atomic and molecular electronic transitions would take place. It must be noted that, regardless of the RF plasma jet as the radiator, two spectral line sets can be recorded in the plasma formed in the Ar/O_2 mixture. The first spectral line set is related to the upper energy states populated by direct electronic (high-energy electrons) collisions with the existing species in the ground state. The second spectral line set is created in collisions between low-energy electrons and argon metastable atoms.

The OES technique is essentially based on the analysis of the light emitted by different species such as neutral or ionised atoms, radicals, or molecules from the plasma discharge medium. Generally, the emission from the gaseous atomic and molecular plasma discharges is used in various optical plasma diagnostic methods. Furthermore, the OES technique is used for the characterisation of the excited species, determination of the photon flux as a function of wavelength, actinometry, and as a diagnostic for the charged particles beam. In OES method, the emission from optically allowed states is insensitive to the beam energy. Moreover, a short lifetime facilitates a good temporal response and fewer complications from quenching. Additionally, in the OES techniques, the resulted excitation by plasma electrons and radiative cascades is minimised by a large amount of excitation energy. Finally, the main advantage of OES technique is that, when the quenching and photon re-absorption in plasma discharge medium are not that much strong, the data interpretation is direct and relatively simple [2–7]. Thus, in this paper, the OES technique is used as an emissive spectroscopy technique for diagnostics of different species formed in a RF plasma jet with Ar/O_2 mixture. The percentage of Ar in the Ar/O_2 mixture is varied. The plasma electron density and excitation temperature are obtained by analysing the obtained optical emission spectra from the discharge media of the RF plasma jet.

2. Experimental set-up

Generally, in biomedical applications, the damaging effects of plasma jet on the human body tissues must be insignificant. Thus, the temperature of the charged particles of the plasma discharge media should be kept relatively small. Fortunately, the temperature of the electrons in the discharge medium of the RF plasma jet is about 1–4 eV. However, the background gas temperature is almost equal to room temperature. Thus, the RF plasma jet devices have to loose heat properly. In addition, the applied power must be reduced [20]. Besides, based on the specific applications, the optimum operational gaseous mixture in the designed RF plasma jet is an important factor. Thus, in this work, the influences of varying the amount of argon in the Ar/O_2 mixture on the performance of the plasma jet are studied.

So far, for various applications of the plasma jets with different power sources and active species, many devices having different power source shapes, geometries, background gases, etc. are developed. Generally, the working gas in the plasma jets can be inert gases (He, Ar or Ne) or mixture of inert gases with molecular oxygen, nitrogen, etc. However, as the existing resources for helium gas are scarce, argon is the preferred gas [21].

The schematic representation of the whole experimental set-up with the typical view of RF plasma jet, gas mixer and spectrometer is shown in figure 1. As depicted in figure 1c, for the designed RF plasma jet, both the central tungsten pin (inner) and aluminum shell (outer) electrodes are powered with the applied RF voltage. The inner electrode is made of a tungsten rod having 1.6 mm diameter and 95 mm length. The outer electrode is made of an aluminum shell with inner and outer diameter of 12 mm and 20 mm, respectively. Moreover, to provide cold dielectric barrier discharge (DBD) plasma between the inner and the outer electrodes, the outer electrode is covered by a quartz tube. The inner and outer diameters of quartz tube are 4 mm and 6 mm, respectively. This device operates at atmospheric pressure in various mixtures of argon and oxygen. Thus, the plasma discharge is formed in a 1.2 mm gap between the inner electrode and the quartz tube. The length of the generated plasma is about 20 mm along the inner electrode. This arrangement for RF plasma jet strongly prevents arcing between the inner and outer electrodes which is particularly unwarranted in biomedical applications.

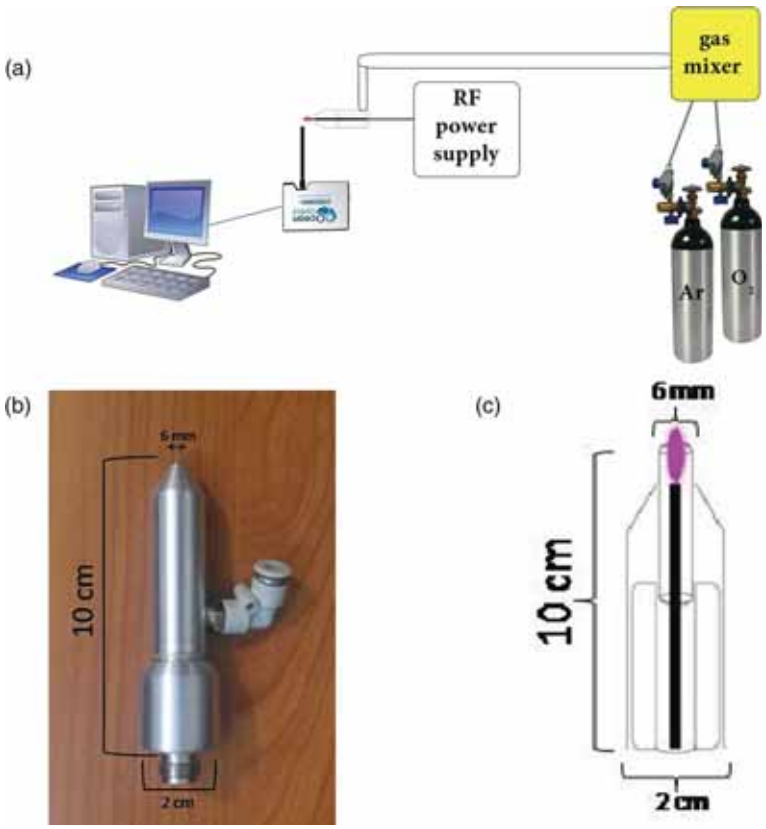

Figure 1. Schematic of (**a**) the experimental set-up with typical view of the RF plasma jet, gas mixer and spectrometer, (**b**) real view of the RF plasma jet and (**c**) interior view of the RF plasma jet.

Such a configuration for the RF plasma jet generates a stable plasma discharge which is produced in the region of the working gas. The produced plasma transfers the reactive species to the processing region, without disturbing the plasma stability. The cold DBD plasma is taken in different fields of technological applications such as biology, materials processing and medicine. Specially, the RF plasma discharge has unique features applications, in plasma medicine such as wound sterilisation, surgical applications, blood coagulation end etc. [22].

In this work, a RFG01BF Basafan power supply with RF fixed-frequency (13.56 MHz) and variable output power (1–100 W) is used. At first, both the output RF power and impedance are varied to reach the most stable plasma jet for all the mixtures of argon and oxygen. The impedance matching network works based on a transmission line matching using the lumped L-type network. It has to be noted that, the L-type matching network is lossless or at least the loss can potentially be made extremely small with the proper component choices. However, the RF input power depends on the application and the sizes of the RF plasma jet. The set-up and the measurement instrumentations are shown in figure 1a.

OES is carried out using a Spectrasuite software and USB2000 Ocean Optic spectrometer. It has a linear CCD and spectral resolution of 0.35 nm. In addition, it stores a full spectrum at every millisecond with a wavelength range sensitivity of 200–1100 nm. Argon is taken as the main carrier gas and is mixed with different percentages of molecular oxygen using a gas mixer.

A photograph of the RF plasma jet in operational conditions in our laboratory is shown in figure 2. This discharge power for the RF plasma jet is fixed at 55 W. It appears uniform to the human eye and, its length can even reach more than 20 mm. The output gas from the gas mixture is injected to the RF plasma jet at a gas flow rate of about 15 SLM (standard litres per minute) which is controlled by a velocity flow controller.

From the practical point of view, the RF plasma jet can move easily and freely in all directions due to its very small size and low weight compared with the RF plasma jets (Babayan *et al* [23] and Weltman *et al* [24]). Moreover, its nozzle design focusses the plasma as a needle. This design is certainly more efficient in localised medical treatments and the surrounding tissues will not get damaged. These features make this RF plasma jet a reliable tool in different fields of medical and industrial applications.

Figure 2. Photograph of the argon RF plasma jet in the operational conditions.

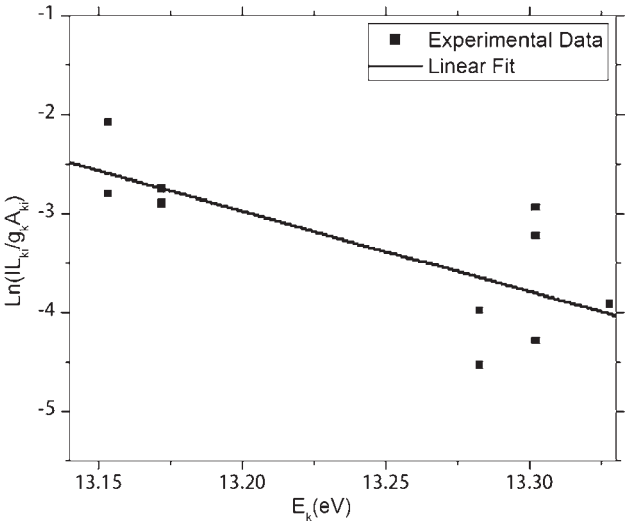

Figure 3. Boltzmann plot for argon excitation temperature.

In this work, using the OES techniques, the excitation temperature and electron density in the discharge medium of the RF plasma jet are estimated. Here, the experimental relative emission intensities of different lines originating from the gaseous atomic and molecular levels are measured. The amount of argon in the Ar/O_2 mixture is varied from 70% to 95%. The obtained spectra from the formed plasma in the RF plasma jet are analysed by Spectrasuite software. The obtained results from OES technique are used to calculate the plasma characteristics of RF plasma jet such as electron excitation temperature and electron density. In order to measure discharge parameters of the RF plasma jet, the intensity of atomic emission lines of the plasma discharge can be used to estimate the population in the electronic levels of argon atom. To this end, the Boltzmann distribution for plasma discharge in the partial local thermodynamic equilibrium (PLTE) conditions must be taken into account. It must be noted that, the non-equilibrium plasmas usually have $T_e > T_{el} > T_v > T_r$ [25,26]. When one or more of these four temperatures are not the same, the system will not be considered in equilibrium or in PLTE conditions. In the experiments performed, the RF plasma jet was in PLTE conditions, where the Maxwell–Boltzmann equilibrium was established. The emission lines from the excited argon species are overabundant and, they have reliable transition probabilities that are published in the literature. Assuming that the upper levels of the selected atomic transitions are in the PLTE conditions, the conventional Boltzmann plot technique can be used to obtain the excitation temperature in the plume of the RF plasma jet.

The emission lines from excited argon and oxygen species are the most abundant, and the reliable transition probability values of these states are published in the literature. Assuming that upper levels of the selected atomic transitions are in the PLTE conditions, the conventional Boltzmann plot technique can be used to determine the excitation temperature in the discharge media of the RF plasma jet. The following relation expresses the relative transition probabilities of two different lines [19,27]:

$$\ln\left(\frac{I\lambda_{ki}}{A_{ki}g_k}\right) = \ln\left(\frac{hcN_0}{4\pi U(T)}\right) - \frac{E_k}{kT_{\text{exc}}}, \tag{1}$$

where I denotes the total intensity, A_{ki} is the transition probability, g_k is the degeneracy of the upper level, λ_{ki} is the wavelength, E_k is the excitation energy and k is the Boltzmann constant. This model assumes that the electron collisions between excited atoms are dominant in the populating and depopulating of the excited atoms.

The well-known Boltzmann plot method is used to measure the excitation temperature. Generally, this method is based on the detection of several plasma emission lines. Thus, the excitation temperature is calculated from the plot of $\ln(I\lambda_{ki}/A_{ki}g_k)$ as a function of E_k (the upper level energy). Hence, using eq. (1), the slope of the fitted plot, i.e., $1/kT_{\text{exc}}$ gives the excitation temperature [28]. Consequently, a linear fit on the Boltzmann plot for a large number of excited levels is shown in figure 3. Additionally, special attentions must be paid for choosing the levels. If the chosen levels are in PLTE condition, the obtained excitation temperatures will be correct. Additionally, the NIST atomic database (table 1) [29] is used to plot eq. (1).

It must be noted that the Stark broadening analysis of the spectral profile of the H_β line which is emitted by the plasma is the most common procedure to measure the electron density (n_e) [25,30,31]. On the other hand, several broadening mechanisms such as natural broadening (this is usually insignificant), Doppler broadening, pressure broadening, and Stark broadening can influence the emission line shape in plasma discharges. Doppler broadening leads to a Gaussian profile, with a FWHM

Table 1. Several spectral parameters of the observed lines for Ar/O_2 mixture (NIST atomic database).

Ion	Wavelength (nm)	$A_{ki} \times 10^7$ (s^{-1})	E_i (eV)	E_k (eV)	Transition	g
ArI	696.543	0.63	11.54	13.32	4p-4s	3
	706.7217	0.38	11.54	13.30	4p-4s	5
	714.7041	0.06	11.54	13.28	4p-4s	3
	727.2935	0.18	11.62	13.32	4p-4s	3
	738.398	0.84	11.62	13.30	4p-4s	5
	750.3868	4.45	11.82	13.47	4p-4s	1
	751.4651	4.02	11.62	13.27	4p-4s	1
	763.5105	2.45	11.54	13.17	4p-4s	5
	772.376	0.51	11.54	13.15	4p-4s	3
	794.8176	1.86	11.72	13.28	4p-4s	3
	800.6156	0.49	11.62	13.17	4p-4s	5
	801.4785	0.92	11.54	13.09	4p-4s	5
	810.3692	2.50	11.62	13.15	4p-4s	3
	811.5311	3.31	11.54	13.07	4p-4s	7
	826.4521	1.53	11.82	13.32	4p-4s	3
	840.8209	2.23	11.82	13.30	4p-4s	5
	842.4647	2.15	11.62	13.09	4p-4s	5
	852.1441	1.39	11.82	13.28	4p-4s	3
	912.2967	1.89	11.54	12.90	4p-4s	3
OI	777.4166	3.69	9.14	10.74	3p-3s	5
	844.6359	3.22	9.52	10.98	3p-3s	5

[30] as follows:

$$\Delta\lambda_D\,(\text{nm}) = 7.16 \times 10^{-7}\lambda\sqrt{\frac{T}{M}} = 3.48 \times 10^{-4}\sqrt{T_g} \quad (2)$$

where $\lambda = 4861.33$ Å is the central wavelength, $M = 1$ g/mol is the atomic weight of H, and T is the temperature of H atoms which is generally equal to the gas temperature T_g (K).

Pressure-broadening phenomenon is due to the perturbation of the energy levels of the emitting atoms in the presence of the surrounding neutral species. Pressure broadening, which leads to a Lorentzian profile, is subdivided into resonance broadening (when emitters and perturbers are of the same type and either the upper or the lower state of the observed line is a resonance level) and van der Waals (vdW) broadening (when emitters are perturbed by neutrals of a foreign gas). In this work, however, the density of H atoms was extremely low. Thus, only van der Waals broadening is taken into the account. The FWHM of the vdW profile is [32–34]

$$\Delta\lambda_P\,(\text{nm}) = 6.8 \times 10^{-3} \cdot \frac{P}{T_g^{0.7}} \quad (3)$$

where P is the gas pressure (Torr) and T_g is in K.

In plasma discharge, the Stark broadening $\Delta\lambda_S$ can be used to estimate plasma electron density (n_e). The hydrogen Balmer series (H_β) is commonly used to measure the plasma electron density without considering the fine structure of the emission line and ion dynamics [35]. The full-width at half-maximum (FWHM) is a parameter which is widely employed to characterise the broadened line profile. Then, the FWHM broadening values of Stark broadening that may affect the H_β line can be calculated. The FWHM of the Stark broadening is related to the electron density via the following relation:

$$\Delta\lambda_S(\text{nm}) = 2 \times 10^{-11}[n_e]^{2/3}, \quad (4)$$

where the plasma electron density is in cm^{-3} [36]. The Stark broadening of the H_β emission line (486.13 nm) gives a reasonable approximation of the plasma electron density.

The parameters of the Voigt profile is given as [34]

$$\Delta\lambda_G = \sqrt{\Delta\lambda_D^2 + \Delta\lambda_{GI}^2}, \quad (5)$$

$$\Delta\lambda_L = \Delta\lambda_P + \Delta\lambda_S, \quad (6)$$

where $\Delta\lambda_G$ and $\Delta\lambda_L$ are FWHM of the Gaussian and Lorentzian components, respectively. In addition, $\Delta\lambda_{GI}$ is the resolution of the experimental apparatus (instrumental broadening).

In this work, in order to perform an accurate deconvolution and to measure the Stark broadening of the spectral line, a fitting code is developed. Both the relevant broadening mechanisms and influences of the fine

structure are implemented in the model. It must be noted that, in this method, the broadening mechanism found for the H_β line as a whole can be extended to the individual fine-structure components. Hence, the Stark and Doppler broadenings can be treated independently. Moreover, the Stark broadening mechanism will not automatically lead to the pure Lorentzian shapes. It must be noted that, there are different broadening mechanisms with a non-negligible contribution to the composed line profiles such as Doppler broadening, pressure broadening and Stark broadening. Therefore, a fitting procedure is needed to do the deconvolution process [37]. The procedure is divided into four steps:

(1) Corrected instrumental profile. Here, the optical system which is used to record the spectrum will cause an extra broadening of spectral lines. This is called instrumental broadening and, it will not depend on the plasma properties. As a first step, the instrumental profile is convoluted with the fine structures forming the corrected instrumental profile.
(2) Calculated profile. This profile is convoluted with a variable Voigt curve forming the calculated complete profile. Thus, in the second step, the contributions of the other broadening mechanisms are introduced. These mainly include Stark and Doppler broadening and, of course, the van der Waals broadening. A variable Voigt curve is used to represent the combined effect of all this broadening mechanisms. Furthermore, in the developed code for fitting process, the Voigt curve is convoluted with the corrected instrumental profile. Hence, the profile is calculated.
(3) Fitting process. The variable Voigt of the calculated profile is then changed until the best fit is obtained with the experimentally measured H_β line. The calculated profile is now compared with the measured H_β line profile. Additionally, using a least squares fitting procedure, the Gaussian and Lorentzian widths of the variable Voigt curve are varied until the best fit is obtained. However, the calculated profile results in an asymmetrical line. Since the instrumental profile is symmetric, this asymmetry is caused by the fine structure.
(4) Stark broadening. Finally, using the fitted Voigt profile, the Stark broadening is obtained. However, the contributions of the other mechanisms are removed. The Voigt curve is obtained from the fitting of experimental data and, only Stark, Doppler and van der Waals (pressure) broadenings contributions are included. However, both the instrumental broadening and fine structure are already considered in the corrected instrumental profile. Besides, using eqs (2) and (3), the Lorentz–van der Waals and Gauss–Doppler contributions are calculated. Then, the Doppler width is removed from the Gaussian part of the fitted Voigt and the van der Waals (pressure broadening) width from the Lorentzian part. The remaining profile is another Voigt curve representing only the Stark contribution. Thus, the FWHM for this Voigt curve is used as the Stark width, $\Delta\lambda_S$. Nevertheless, it is often assumed that the Stark profiles are purely Lorentzian [37].

Hence, by comparing the Voigt profile and the measured emission lines, the FWHM of Stark broadening can be obtained. Besides, the plasma electron density is obtained when a best fit between the two profiles is performed [35,36]. The emission intensities of all the peaks are significantly increased with the amount of Ar in the Ar/O_2 mixture.

3. Results and discussions

In this work, by applying RF power to the manufactured plasma jet (figure 1), gas breakdown occurs. Consequently, charged particles such as electrons, ions, and neutral atoms are produced in the plasma discharge medium of the RF plasma jet. The ionised state in the gas atoms and molecules builds up until it reaches appreciable values, and plasma species start to radiate at different wavelengths. To recognise the discharge species, the obtained spectra from the OES technique for the RF plasma jet and with different mixtures of argon and oxygen gases at the atmospheric pressure are used. Owing to different medical applications of plasma discharges, the plasma sources generally developed for biomedical applications are typically designed to generate, at atmospheric pressure and medium density, low-temperature discharge that is suitable for the direct treatment of thermally liable living substrates [36].

The obtained spectra are normalised with response and transmission curves of the spectrometer and optical fibre that is provided by the spectrometer manufacturer. Generally, in order to truly establish the importance of the species roles in various processing parameters, the area under each OES spectrum is integrated [38].

It is worthy to mention that, based on the ionisation rate for atmospheric plasma discharges, most of the plasma energy is spent on the production of optically allowed states, forbidden states (metastable), and dissociation. Most of the metastable species have long lifetimes. Thus, the metastable population can grow to high levels. Strong emissions from the excited neutral atoms are predominant for argon (ArI). The optical emission comes mainly from depopulation of the 4p levels via the multiple 4p–4s transitions.

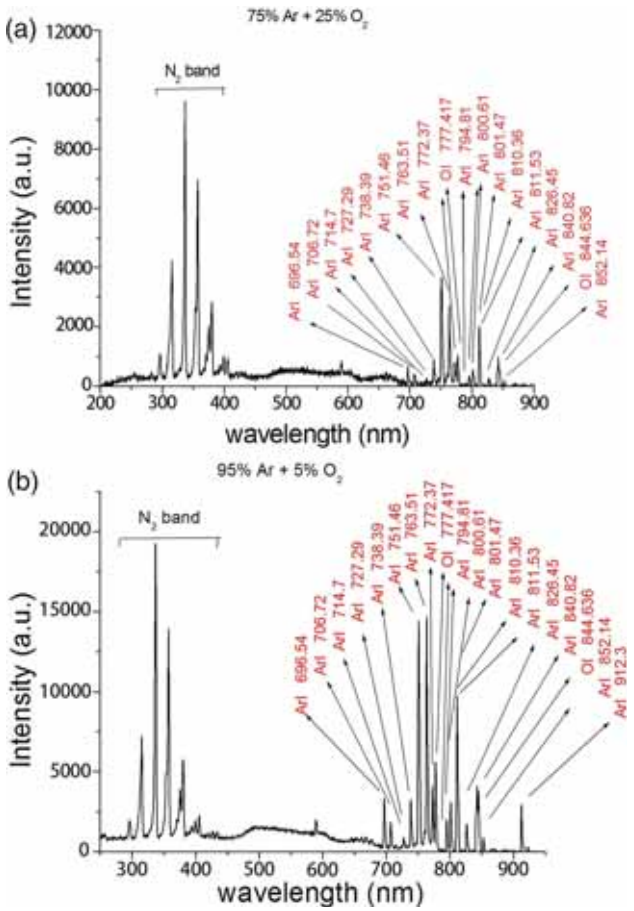

Figure 4. The obtained spectra from the RF plasma jet for different percentages of Ar in Ar/O_2 mixture.

Figure 4 shows the main emission peaks corresponding to several transition lines of atomic oxygen and argon. The emission lines with highest intensities in the discharge medium of the plasma jet are related to argon (ArI, 4p→4s, 690–912 nm), N_2 emission bands ($C^3\Pi_u \rightarrow B^3\Pi_g$, 300–440 nm) and atomic oxygen (OI, 777.4 and 844 nm).

In the argon plasma discharge, the highest emission intensities of the neutral argon atom (ArI) have been recorded in the wavelength range of 750–850 nm. The mechanism for exciting the $4p_0$ level of Ar is the one-step electron impact excitation from the ground state. Additionally, in most of the measured lines, maximum values of the radiation intensity of Ar 4p→4s transitions at higher percentages of argon in Ar/O_2 mixture will increase. This is owing to direct effects of electron density on the excitation rate of Ar atoms to the 4s state. This is again due to the higher ionisation rate at higher percentages of argon in Ar/O_2 mixture and its direct influence on the electron excitation temperature in the RF plasma jet. Since the number density of the excited Ar atoms at the higher percentages of argon in Ar/O_2 mixture is higher, the emission intensities from argon ion increase with the amount of Ar in the mixture.

Furthermore, in the oxygen plasma discharges, many peaks associated with the optical transitions of the atomic oxygen (O) are observed. As observed in figure 4 for radiation emission intensity, the corresponding atomic oxygen peaks mainly occur at 777.4 nm ($3p_2 \rightarrow 3s_2$) and 844.6 nm ($3p_2 \rightarrow 3s_1$). The highest intensity corresponds to the 777.4 nm emission line. Based on the Ar* reaction with molecular oxygen, $Ar^* + O_2 \rightarrow Ar + O + O$, the quenching reaction of the metastable argon (Ar^*) with O_2 results in an increase in atomic oxygen (O) with respect to O_2 molecules. The lifetimes of electrons in resonant, metastable, allowed and forbidden excited energy states are determined by many factors which could be quite different from the theoretical approaches. However, in plasma discharge media, the microscopic processes are governed by the collective interactions [20].

It must be noted that, due to the open air existence in the discharge medium of the plasma jet, the quenching mechanisms for the excited species are quite different [39]. Although air molecules can diffuse into the nozzle, which is indicated by the N_2 bands, the air concentration was considered to be very low and would not play an important role in the quenching processes of the excited and metastable Ar atoms inside the nozzle.

To determine the excitation temperature, T_{exc}, from eq. (1) under the Boltzmann approximation, the neutral argon and oxygen emission lines are obtained from NIST and listed in table 1 [29], where E_k and E_i are the energies of the upper and lower levels of the radiative transitions, respectively.

Generally, to understand the cross-linkage among plasma discharge species, an energy diagram of the spectral emission must be produced. Furthermore, the lifetimes of electrons in the metastable energy levels are much shorter than in the ordinary excited energy levels and, they are many orders of magnitude shorter than the lifetime of electrons at metastable energy levels. Plasma charged particle kinetics at the atmospheric pressure could be impacted by quenching among the argon metastables. The main mechanism of excitation or de-excitation of argon 4s energy states is the direct electron excitation from the ground level and deactivation of the Ar(4p) state. The Ar(4p) states only get relaxed into Ar(4s) states by radiative emission. Deactivation of Ar(4p) to the ground state is improbable and does not occur appreciably [40]. There is a direct relation between the production of excited oxygen atoms and the plasma discharge density. Two main oxygen spectral emissions (i.e., 777.4 nm, 844.6 nm) would occur. The upper energy levels for both emission lines can be populated by the direct electron impact (excitation process)

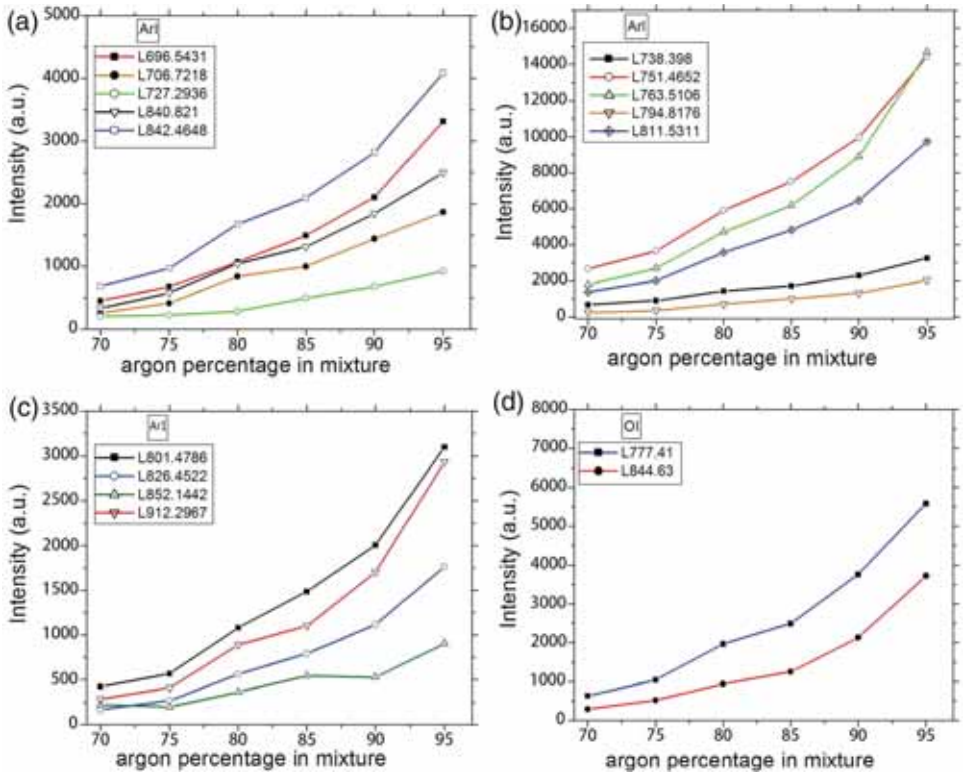

Figure 5. (**a**, **b** and **c**) Neutral argon atom spectra peaks and (**d**) neutral oxygen atom spectra peaks vs. Ar percentage in the Ar/O_2 mixture.

from the ground state of OI. Moreover, at higher argon gas flow rates, the concentration of molecular oxygen and oxygen radicals drastically decreases. Additionally, the creation of O777 and O844 is significantly influenced by the argon metastable atoms.

Influences of argon percentage in the Ar/O_2 mixture on the spectral intensity (ArI and OI) of the RF plasma jet is shown in figure 5. As seen, increase in the Ar percentage causes the emission intensity from O atoms to be slightly increased. In addition, by increasing the argon percentages, the line intensities from Ar atoms and O atoms almost linearly increase presumably due to the enhancement of excitation frequency which is increased by the energetic electrons in the plasma discharge medium. The spectroscopic features of RF and DC plasma discharges with the Ar/O_2 mixture at 50 Pa gas pressure were studied by Pavlik *et al* [41]. Their findings show that, at the higher flow rates of O_2, the spectral intensities for RF discharge will increase. Furthermore, Lock *et al* [42] showed that, at higher O_2 concentration in Ar/O_2 mixture, while the intensity of the emitted spectra from oxygen increases, the emitted spectra from argon would decrease.

The specific spectral line of H_β that is emitted spontaneously from the plasma is employed to estimate the electron density by analysing the full-width at half-maximum (FWHM) in the Stark broadening ($\Delta\lambda_S$). However, owing to the fast collisions among the plasma discharge particles in the atmospheric pressure, several broadening mechanisms could be appeared. They mainly include the Stark (caused by collisions among charged particles), Van der Waals (due to the collisions of neutral particles), Doppler (effect of the thermal motion of emitting atoms) and natural broadenings. Each broadening mechanism would cause an energy level shifting of the emitting atoms and the relative importance of these broadenings is determined by the plasma conditions. Thus, in comparison with the other broadening mechanisms, the resonance and natural broadening can be ignored in the atmospheric pressure plasma discharges. On the other hand, the Doppler broadening, $\Delta\lambda_D$, is normally caused by the random thermal motion of the emitting atoms and, it depends on the gas temperature, T_g. The approximate formula for FWHM is given by eq. (2). Moreover, the Doppler broadening has a Gaussian shape which can be obtained from eq. (5). In addition, as the excited atoms interact with the neutral ground-state atoms of other species, the Van der Waals broadening, $\Delta\lambda_{vdW}$, is an important broadening mechanism in high pressure plasmas and, thus, FWHM can be calculated using eq. (3). Besides, the Stark broadening has a Lorentz profile which can be obtained from eq. (6). However, the convolution of the Gaussian and Lorentz profiles gives a Voigt profile. It

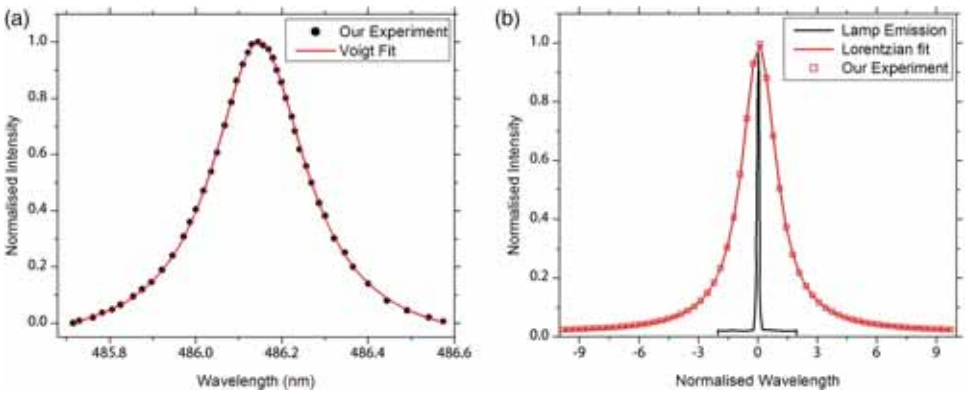

Figure 6. (**a**) Experimental data of the H_β line fitted to a Voigt profile and (**b**) comparison of Stark-broadened profile and a low pressure discharge lamp.

Table 2. Typical broadening values for different electron densities.

Ar percentage in the Ar/O_2 mixture	$\Delta\lambda_L$ (nm)	$\Delta\lambda_{vdW}$ (nm)	$\Delta\lambda_S$ (nm)	Electron density ($\times 10^{14}$ cm^{-3})
70	0.0567	0.0927	0.0567	1.51
75	0.0711	0.0934	0.0711	2.12
80	0.0949	0.0936	0.0949	3.27
85	0.1319	0.0938	0.1319	5.36
90	0.1630	0.0940	0.1630	7.36
95	0.1794	0.0942	0.1794	8.50

must be noted that, FWHM of the Stark broadening is related to the electron density via eq. (4) [43]. A comparison between the performed experiments and Voigt profile is presented in figure 6a.

Figure 6b shows the profiles corresponding to the normalised obtained intensity and a low pressure discharge lamp vs. the wavelength (normalised). Moreover, a Lorentzian fit is performed on the obtained experimental data. It must be noted that, for the low pressure lamps, the emission lines are limited to a Doppler-broadened profile with a very narrow FWHM [35].

Lorentz broadening ($\Delta\lambda_L$), van der Waals broadening ($\Delta\lambda_{vdW}$) and Stark broadening ($\Delta\lambda_S$) at the atmospheric pressure for different typical electron densities are presented in table 2.

Based on eqs (1) and (4), the excitation temperature and electron density for each spectrum in Ar/O_2 mixture are calculated and presented in table 3. As the amounts of Ar is lower in the Ar/O_2 mixture, the number density of the excited atomic OI increases. However, when argon in the Ar/O_2 mixture increases, the Penning excitation and Penning dissociation of argon will increase the number density of the excited states of O, O_2 and O_2^+.

Variations of the excitation temperature and electron density of the plasma discharge in the RF plasma jet in terms of argon percentage in the Ar/O_2 mixture are shown in figure 7. As seen in figure 7a, increase

Table 3. Excitation temperature and electron density of various percentages of Ar in the Ar/O_2 mixture.

Ar percentage in the Ar/O_2 mixture	Excitation temperature (eV)	Electron density ($\times 10^{14}$ cm^{-3})
70	1.92 ± 0.12	1.51
75	1.84 ± 0.02	2.12
80	1.73 ± 0.13	3.27
85	1.46 ± 0.08	5.36
90	1.11 ± 0.04	7.36
95	0.86 ± 0.07	8.50

in the argon percentage in the mixture resulted in the decrease of the excitation temperature. This must be due to the decrease in energy loss by the electrons during ionising collision with O_2 molecules as the ionisation cross-section for O_2 is smaller than that of argon [11]. Furthermore, as seen in figure 7b, at higher argon percentages in the Ar/O_2 mixture, the electron density is increased. Besides, owing to the enhancement of electron attachment in the mixture, the plasma electron density reduces at higher oxygen contributions (lower argon contributions) in the mixture. Hence, increase in electron density in the plasma discharge medium will reduce their mean free path. This reflects in the reduction

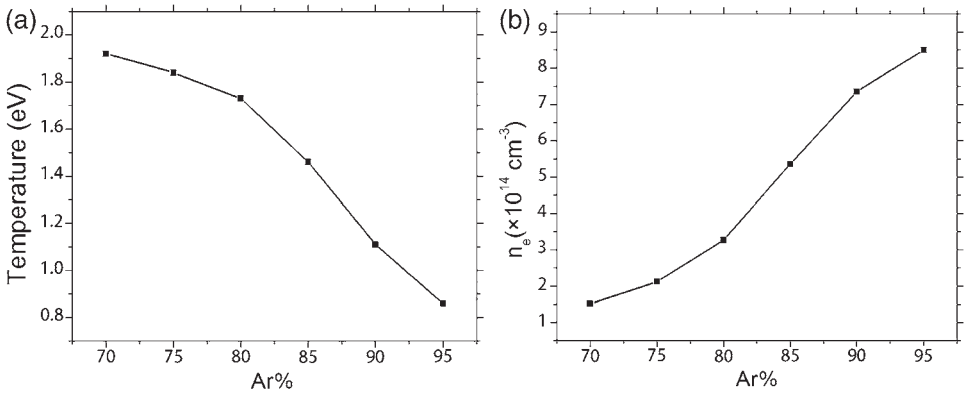

Figure 7. Variation of the (**a**) excitation temperature and (**b**) density of plasma electron vs. the Ar percentage in Ar/O_2.

in acceleration of the electrons inside the plasma discharge medium of the RF plasma jet. Thus, their kinetic energy (electron temperature) would be decreased. This is in agreement with the experimental findings by Chung *et al* [15] for 40 mTorr and 500 W. Furthermore, in an experimental study by Khalaf *et al* [16] on the evolution of temperature in a DC plasma jet for 0.14 mbar and a 1400 V DC power supply it was shown that the temperature increases with increasing O_2 percentage in the mixture. Hence, the plasma jet could be suitable for medical and surgical applications. Plasma generated from argon and oxygen mixture is in agreement with the experimental findings by Pan *et al* [44]. In their work, the premixed argon and oxygen (98% Ar and 2% O_2 per volume) was used as a working gas to evaluate the treated tooth biofilms.

As the ion species formed from argon atoms have lower ionisation potential, their mixture with oxygen results in an increase in electron density at higher volumetric ratios of the argon ion species. Besides, when argon is mixed with the oxygen plasma, the temperature of the electron would be lower and the degree of oxygen dissociation increases. The obtained wavelength-resolved optical emission profiles for the emission of spectral lines of argon show that the both the free electrons and argon metastable atoms have important influences on the overall spectral emission.

For the Ar/O_2 mixture plasma under 50 mTorr pressure, Lock *et al* [42] obtained the optical emission spectrum in the wavelength range of 600 nm–950 nm. The maximum intensities of the spectra in 70% and 90% of argon in Ar/O_2 mixture were reported to be 400 and 350 in arbitrary units (a.u.), respectively. It must be noted that, the experimental findings presented in this work for the optical emission spectrum are in the wavelength range of 290 nm–950 nm. Moreover, the maximum intensities of the spectra in 70% and 90% of argon in Ar/O_2 mixture are 13000 and 15000 in a.u., respectively. However, the observed difference between our findings and the obtained results of Lock *et al* [42] for the wavelength range of 290 nm–950 nm might be due to the operational pressure, as the gas pressure in the performed experiment in this work is kept at 760 Torr. Additionally, as shown in figure 4, the detected UV emission spectrum from the RF plasma jet is clearly visible. The UV spectrum ranges from 290 nm to 400 nm, which does not affect the human body DNA. In addition, UV impact on human skin is particularly studied in dermatology [23,45]. There are several effects of UV light on the skin, both indirect effects from the formation of free radicals and direct cellular injury.

Finally, as the obtained spectrum intensity at higher percentages of argon in the mixture is increased, the number of reactive plasma species are higher. Thus, this device can be used for sterilisation and for cancer therapy applications. On the other hand, at lower argon percentages in the Ar/O_2 mixture, the excitation temperature is higher. It can be concluded that, in such an operational condition, the plasma jet is suitable in surgical applications.

4. Conclusions

In this work, the optical emission spectra obtained from the excited atomic Ar are analysed. To this end, the percentage of Ar in the Ar/O_2 mixture in the RF DBD plasma jet is varied from 70% to 95%. The excitation temperature and electron density of the designed RF plasma jet are obtained. In the operational working condition of the RF plasma jet with only argon, the highest emission intensities of the neutral argon atom (ArI) were recorded in the wavelength range of 750–850 nm. It was observed that, at most of the measured lines, the radiation intensity of Ar 4p→4s transitions is higher when the amount of Ar in Ar/O_2 mixture is higher. On

the other hand, increasing the Ar percentage results in higher emission intensities from O atoms and, there is a linear increase in the line intensities from Ar atoms and Ar ions including O atoms. Moreover, for the optical transitions of O atom, the highest intensity occurs at the 777.4 nm emission line. It was seen that the quenching of Ar* with O_2 causes the atomic oxygen to increase with respect to O_2 molecules. Finally, higher percentage of Ar in the mixture causes a decrease in the excitation temperature and increase in the electron density.

Acknowledgements

The authors would like to acknowledge the Institute of Science and High Technology and Environmental Sciences for financial support (No. 7.S.95.3422-22/12/1395).

References

[1] M J Shenton and G C Stevems, *J. Phys. D: Appl. Phys.* **34**, 2761 (2001)
[2] W T Huang and S Z Li, *IEEE Trans. Plasma Sci*. **38**, 121 (2010)
[3] N Abramzon, J C Joaquin, J Bray and G Brelles-Marino, *IEEE Trans. Plasma Sci.* **34**, 1304 (2006)
[4] X T Deng, J J Shi and M G Kong, *IEEE Trans. Plasma Sci.* **34**, 1310 (2006)
[5] X H Zhang, J Huang and X D Liu, *J. Appl. Phys.* **105**, 302 (2005)
[6] M Laroussi and X Lu, *Appl. Phys. Lett*. **87**, 902 (2005)
[7] S Tao, Z Cheng, L Kaihua, Z Dongdong, W Jue, Y Ping and Z Yuanxiang, *Appl. Surf. Sci.* **12**, 3888 (2010)
[8] S Tao, Y Yang, Z Cheng, J Hui, Y Ping and Z Yuanxiang, *Plasma Sci. Technol*. **13**, 735 (2011)
[9] S Tao, Z Cheng, N Zheng, Y Yang, Y Ping and Z Yuanxiang, *Plasma Sci. Technol.* **13**, 591 (2011)
[10] M A Lieberman and A J Lichtenberg, *MRS Bull.* **30**, 899 (2005)
[11] L Moravský, M Klas, S Matejcik and E Machova, *Proceedings of the 22nd Annual Conference of Doctoral Students*, 149 (2013)
[12] L Schaper, S Reuter, J Waskoenig, K Niemi, V Schulz-von der Gathen and T Gans, *J. Phys.: Conf. Ser.* **162**, 012013 (2009)
[13] H Tanaka *et al*, *IEEE Trans. Plasma Sci.* **1**, 3813 (2014)
[14] C Hoffmann, C Berganza and J Zhang, *Med. Gas Res*. **3**, 21 (2013)
[15] T H Chung, H R Kang and M K Bae, *Phys. Plasmas* **19**, 113502 (2012)
[16] M K Khalaf, I R Agool and S H Abd Muslim, *Int. J. Appl. Innov. Engng. Manage.* **3**, 113 (2014)
[17] S Ono, T Suganuma and Y Suzuki, *19th International Symposium on Plasma Chemistry* (Bochum, 26–31 July 2009)
[18] K Wagatsuma and H Kichinosuke, *Anal. Chim. Acta* **306**, 193 (1995)
[19] J Ying, R Chunsheng, Y Liang, Z Jialiang and W Dezhen, *Plasma Sci. Technol.* **15**, 1203 (2013)
[20] P J Cullen and V Milosavljevi, *Prog. Theor. Exp. Phys*. **2015**(**1**), 063J01 (2015)
[21] J Florian, N Merbahi, G Wattieaux, J-M Plewa and M Yousfi, *IEEE Trans. Plasma Sci.* **43**, 3332 (2015)
[22] M Laroussi, *Plasma Sci.* **37**, 714 (2009)
[23] S E Babayan, J Y Jeong, A Schutze, V J Tu, M Moravej, G S Selwyn and R F Hicks, *Plasma Sources Sci. Technol*. **10**, 573 (2001)
[24] K D Weltmann, E Kindel, R Brandenburg, C Meyer, R Bussiahn, C Wilke and T von Woedtke, *Contrib. Plasma Phys*. **49**, 631 (2009)
[25] C O Laux, T G Spence, C H Kruger and R N Zare, *Plasma Sources Sci. Technol*. **12**, 125 (2003)
[26] D Staack, B Farouk, A Gutsol and A Fridman, *Plasma Sources Sci. Technol.* **14**, 700 (2005)
[27] S Pandhija and A K Rai, *Appl. Phys. B* **94**, 545 (2009)
[28] M C Quintero, A Rodero, M C Garcia and A Sola, *Appl. Spectrosc.* **51**, 778 (1997)
[29] https://physics.nist.gov/PhysRefData/ASD/lines_form.html
[30] H R Griem, *Plasma spectroscopy* (McGraw-Hill, New York, 1964)
[31] J Torres, M J van de Sande, J van der Mullen, A Gamero and A Sola, *Spectrochim. Acta B* **61**, 58 (2006)
[32] M A Gigosos and V Cardenoso, *J. Phys. B* **29**, 4795 (1996)
[33] F J Mehr and M A Biondi, *Phys. Rev.* **176**, 322 (1968)
[34] S G Belostotskiy, T Ouk, V M Donnelly, D J Economou and N Sadeghi, *J. Appl. Phys.* **107**, 053305 (2010)
[35] A Yu Nikiforov, Ch Leys, M A Gonzalez and J L Walsh, *Plasma Sources Sci. Technol.* **24**, 034001 (2015)
[36] M Qian, C Ren, D Wang, J Zhang and G Wei, *J. Appl. Phys.* **107**, 063303 (2010)
[37] J M Palomares, S Hubner, E A D Carbone, N de Vries, E M van Veldhuizen, A Sola, A Gamero and J J A M van der Mullen, *Spectrochim. Acta B* **73**, 39 (2012)
[38] V Milosavljevic and G Poparic, *Phys. Rev. E* **63**, 036404 (2001)
[39] Q Xiong, A Y Nikiforov, X P Lu and C Leys, *J. Phys. D: Appl. Phys*. **43**, 415201 (2010)
[40] R S F Chang and D W Setser, *J. Chem. Phys.* **69**, 3885 (1978)
[41] J Pavlik, R Hrach, P Hedbavny and P Sovièek, *Superficies Vacio*. **9**, 131 (1999)
[42] E H Lock, R F Fernsler, S Slinker and S G Walton, Naval Research Laboratory Report (2011)
[43] D Xiao, C Cheng, J Shen, Y Lan, H Xie, X Shu, Y Meng, J Li and P K Chu, *Phys. Plasmas* **21**, 053510 (2014)
[44] J Pan *et al*, *Cold Plasma Therapy* **39**, 105 (2013)
[45] M K Boudam, M Moisan, B Saoudi, C Popovici, N Gherardi and F Massines, *J. Phys. D: Appl. Phys*. **29**, 3494 (2006)